



Synthesis and biological evaluation of novel imidazo[1,2-*a*]pyridine-oxadiazole hybrids as anti-proliferative agents: Study of microtubule polymerization inhibition and DNA binding

Dilep Kumar Sigalapalli^a, Gaddam Kiranmai^b, G. Parimala Devi^c, Ramya Tokala^a, Sravani Sana^a, Chaturvedula Tripura^b, Govinda Shivaji Jadhav^a, Manasa Kadagathur^a, Nagula Shankaraiah^{a,*}, Narayana Nagesh^{b,*}, Bathini Nagendra Babu^{c,*}, Neelima D. Tangellamudi^{a,*}

^a Department of Medicinal Chemistry, National Institute of Pharmaceutical Education and Research (NIPER), Hyderabad 500037, India

^b CSIR-Centre for Cellular and Molecular Biology, Medical Biotechnology Complex, ANNEXE II, Uppal Road, Hyderabad 500007, India

^c Department of Fluoro-Agrochemicals, CSIR-Indian Institute of Chemical Technology, Hyderabad 500007, India

ARTICLE INFO

Keywords:

Imidazo[1,2-*a*]pyridine
1,3,4-oxadiazole
Cytotoxicity
Apoptosis
Tubulin polymerization
Molecular docking
ADME/T

ABSTRACT

Efforts towards the development of potential anticancer agents, a new series of imidazo[1,2-*a*]pyridine-oxadiazole hybrids were synthesized and evaluated for their *in vitro* anticancer activity against lung cancer (A549) and prostate cancer (PC-3, DU-145) cell lines. Amongst the compounds tested, **6d** showed the highest potency on A549 cells with an IC₅₀ value of 2.8 ± 0.02 μM. Flow cytometric analysis of compound **6d** treated A549 cells showed apoptosis induction by annexin-v/PI dual staining assay and the effect of **6d** on different phases of cell cycle was also analyzed. Target based studies demonstrated the inhibition of tubulin polymerization by **6d** at an IC₅₀ value of 3.45 ± 0.51 μM and its effective binding with CT-DNA. Further, the molecular modelling studies revealed that **6d** has a prominent binding affinity towards α/β-tubulin receptor with admirable physico-chemical properties.

1. Introduction

Cancer is the second most deadly disease after cardiovascular diseases. Cancer is known as a worldwide killer for the last few decades. It is a life-threatening disease, which is the result of abnormal cell cycle and apoptosis regulation, characterized by uncontrolled cell growth and cell division.^{1–3} Effective cancer treatment with fewer side effects is the major topic of research in the pharmaceutical industry and academia for the last few decades.⁴ In this vision, microtubule modulators have played an essential role in cancer chemotherapy over the past decades.^{5,6} In this connection, the development of chemotherapeutic agents that inhibit the function of tubulin leads to metaphase arrest, and DNA binding ability will ultimately help in the activation process of apoptosis.^{7,8}

Imidazo[1,2-*a*]pyridines are fused bicyclic 5–6 membered heterocycles with a wide range of pharmacological activities such as antiviral,

antifungal, antibacterial, hyposensitive, antiprotozoal, anti-inflammatory and anticancer, etc.⁹ Imidazo[1,2-*a*]pyridines are also good bioisosteres for indoles and azaindoles. Some of the marketed drugs such as zolpidem, necopidem, minodronic acid and zolimidine consist of imidazo[1,2-*a*]pyridine as core moiety.¹⁰ In the recent years, a variety of imidazo[1,2-*a*]pyridine containing molecules were reported as promising anticancer agents, in particular, imidazo[1,2-*a*]pyridines substituted at C2 and C3 position showed remarkable anticancer activity.^{11,12} Imidazo[1,2-*a*]pyridines show anticancer activity via acting on CDK, VEGFR, PI3K, EGFR, topoisomerase IIα, micro-tubulin protein, etc.^{13–15} Weiteng *et al.* reported novel 2-phenyl-imidazo[1,2-*a*]pyridine analogs that act as anti-proliferative agents by inhibiting tubulin polymerization.¹⁶ Recently, Kamal *et al.* synthesized new curcumin inspired imidazo[1,2-*a*]pyridine analogs as tubulin polymerization inhibitors.¹⁷

On the other side, oxadiazole is one of the important structural components in several pharmaceutical products. Among all the

* Corresponding authors.

E-mail addresses: shankar@niperhyd.ac.in (N. Shankaraiah), nagesh@ccmb.res.in (N. Nagesh), bathini@iict.res.in (B.N. Babu), tdneelima@gmail.com (N.D. Tangellamudi).

<https://doi.org/10.1016/j.bmc.2021.116277>

Received 10 April 2021; Received in revised form 7 June 2021; Accepted 9 June 2021

Available online 16 June 2021

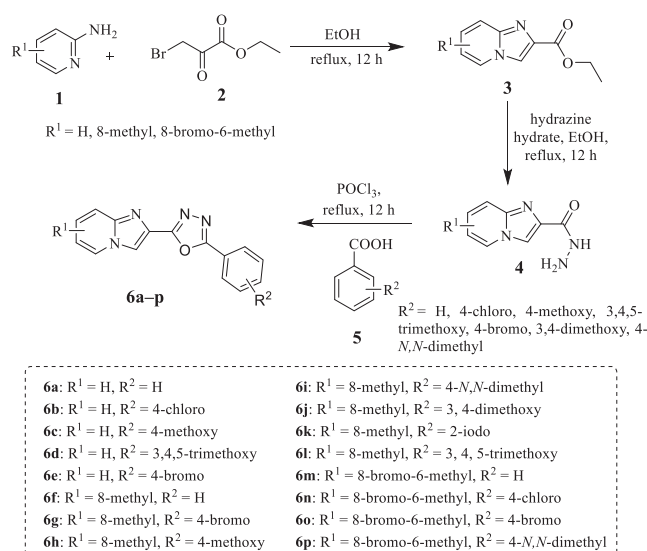
0968-0896/© 2021 Elsevier Ltd. All rights reserved.

oxadiazole isoforms, 1,3,4-oxadiazole displays good stability, remarkable hydrogen-bonding capability with receptor/drug target and contributes to the lipophilicity of the drug, thus providing an easy access to the drug target.¹⁸ The azole functionality in the 1,3,4-oxadiazole is responsible for diversified biological activities such as hypoglycemic, antidepressant, antitubercular, anti-anxiety, anticancer, antifungal, antibacterial and anti-inflammatory, etc.¹⁹ Zibotentan, raltegravir and furamizole are some established drugs that contain 1,3,4-oxadiazole scaffold.²⁰ 1,3,4-Oxadiazoles act as a potential anticancer agents by inhibiting the different enzymes which are essential for cell growth, such as telomerase, histone deacetylase (HDAC), topoisomerase, epidermal growth factor (EGF), vascular endothelial growth factor (VEGFR), etc.²¹ In recent years, Vaidya *et al.* published a review on recent progress in anticancer activities of 1,3,4-oxadiazole and its derivatives.²² Kamal *et al.* reported combretastatin-linked 1,3,4-oxadiazole conjugates and 2-anilinicotinyl-linked 1,3,4-oxadiazole derivatives as potent tubulin polymerization inhibitors.^{23,24}

In the past few decades, molecular hybridization has been an important technique used in medicinal chemistry to develop molecular hybrids with enhanced biological activities by combining two or more pharmacophores/scaffolds. The challenges associated with the present drugs such as selectivity, specificity and multidrug resistance may be circumvented by molecular hybridization technique for the development of molecular hybrids as anticancer agents.²⁵ Earlier, we reported various biologically active molecular hybrids as tubulin inhibitors.^{26–28} In continuation of our efforts in the direction of the development of bioactive tubulin inhibitors, we designed and synthesized certain imidazo[1,2-*a*]pyridine-1,3,4-oxadiazole hybrids by linking imidazo[1,2-*a*]pyridine with 1,3,4-oxadiazole by using the hybridization technique (Fig. 1), and further evaluated them for *in vitro* anticancer activity.

2. Chemistry

To achieve the designed molecules, we began with the condensation of 2-aminopyridines (**1**) with ethyl bromo pyruvate (**2**) in ethanol, which resulted in ethyl imidazo[1,2-*a*]pyridine-2-carboxylate (**3**) followed by reaction with hydrazine hydrate to get imidazo[1,2-*a*]pyridine-2-carbohydrazide intermediate **4** with good yields.^{17,29} Finally, the oxidative cyclization between imidazo[1,2-*a*]pyridine-2-carbohydrazide (**4**) and aromatic acids **5** in the presence of POCl₃ yielded imidazo[1,2-*a*]pyridine-1,3,4-oxadiazole hybrids **6a–p** in good to excellent yields (Scheme 1).²⁹ The synthesized analogs were characterized by utilizing HRMS, ¹H and ¹³C NMR spectroscopic techniques. The ¹H NMR spectrum of the representative compound **6d** showed a singlet of imidazopyridine at δ 8.98 and a sharp singlet of the two aromatic protons belonging to the trimethoxy benzene ring at δ 7.57. The protons



Scheme 1. Synthesis of imidazo[1,2-*a*]pyridine-1,3,4-oxadiazole hybrids **6a–p**.

corresponding to the methoxy groups appeared at δ 4.12 and 4.09 and the rest of the aromatic protons appeared in the range of δ 8.87–7.69. In ¹³C NMR of **6d**, the carbons of 1,3,4-oxadiazole fragment gave two peaks at δ 167.12 and 155.16. While the two aromatic carbons (C3 and C5) of the trimethoxy benzene motif attached the methoxy groups gave a peak at δ 153.7, the carbon – C4 gave a peak at 137.7. The C2 and C6 carbons the benzene ring gave a peak at 105.5. The bridged carbon and the C3 carbon of the imidazopyridine gave peaks at δ 141.4 and 112.2, respectively. The ether carbons of the trimethoxy group gave peaks at 60.89 and 55.7.

3. Pharmacology

3.1. *In vitro* antiproliferative activity

The synthesized imidazo[1,2-*a*]pyridine-1,3,4-oxadiazole hybrids **6a–p** were screened for their *in vitro* cytotoxicity against a panel of human cell lines such as lung cancer (A549), prostate cancer (PC-3, DU-145) and normal embryonic kidney (HEK-293) using 3-(4,5-dimethylthiazol-2-yl)-2,5-diphenyl tetrazolium bromide (MTT) assay.³⁰ The IC₅₀(μ M) values of compounds **6a–p** and reference standard are displayed in Table 1. The initial cytotoxic results indicated that some of the imidazo[1,2-*a*]pyridine-1,3,4-oxadiazole hybrids exhibit moderate to

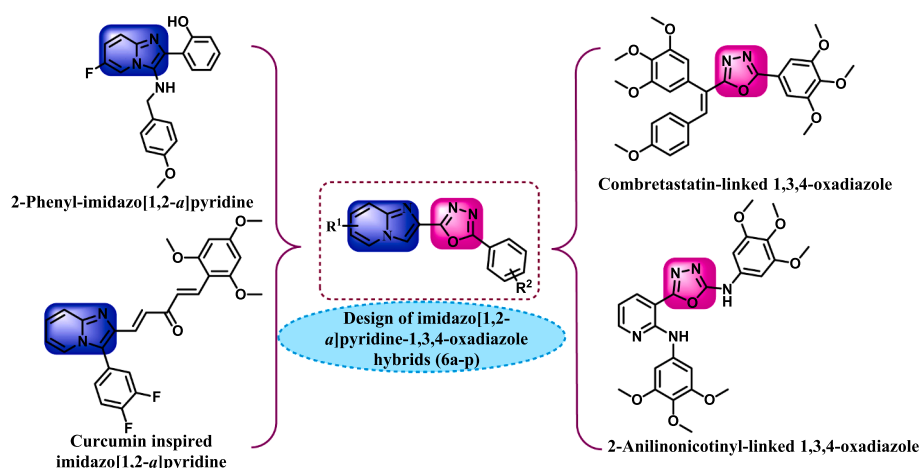


Fig. 1. Examples of bioactive imidazo[1,2-*a*]pyridine and 1,3,4-oxadiazole-containing tubulin polymerization inhibitors.

Table 1
In vitro anticancer activity of compounds **6a-p**.

Compound	IC ₅₀ (μM) ^a			
	A549 ^b	PC-3 ^c	DU-145 ^d	HEK-293 ^e
6a	23.4 ± 0.12	22.2 ± 0.14	23.4 ± 0.23	–
6b	32.4 ± 1.2	33.7 ± 0.34	32.8 ± 0.89	–
6c	11.9 ± 0.01	13.4 ± 0.13	12.9 ± 0.13	–
6d	2.8 ± 0.02	3.5 ± 0.12	4.5 ± 0.2	89 ± 1.23
6e	>50	>50	>50	–
6f	23.4 ± 0.56	22.8 ± 0.99	21.8 ± 0.89	–
6g	34.7 ± 0.56	37.8 ± 0.67	38.9 ± 0.78	–
6h	12.8 ± 0.43	11.8 ± 0.12	10.8 ± 0.11	–
6i	12.3 ± 0.12	11.6 ± 0.24	10.8 ± 0.23	–
6j	10.9 ± 0.02	11.5 ± 0.22	11.8 ± 0.45	–
6k	33.4 ± 0.24	33.5 ± 0.21	31.5 ± 0.12	–
6l	9.9 ± 0.23	10.9 ± 0.13	11.2 ± 0.13	–
6m	14.5 ± 0.25	17.8 ± 1.4	18.9 ± 1.54	–
6n	43.5 ± 1.2	42 ± 0.23	46 ± 1.1	–
6o	23.4 ± 1.5	24.5 ± 0.75	22.3 ± 0.67	–
6p	10.8 ± 0.12	11.2 ± 0.56	12.8 ± 0.13	–
Podophyllotoxin	0.09 ± 0.01	0.06 ± 0.89	0.06 ± 0.08	–

^a 50% Inhibitory concentration after 48 h of drug treatment.

^b Human lung cancer.

^{c, d} Human prostate cancer.

^e Human normal embryonic kidney.

good cytotoxic activity against the tested cancer cells with IC₅₀ values in the range of 2.8 ± 0.02 to 18.9 ± 1.54 μM.

The preliminary screening results indicated that compounds **6c**, **6d**, **6h**, **6i**, **6j**, **6l** and **6p** were the most active, the remaining are moderately active to less active against the tested cancer cells. Captivatingly, the compound **6d** was found to be most active in the lung (A549) and prostate (PC-3, DU-145) cell lines and showed distinct cytotoxic activity with IC₅₀ of 2.8 ± 0.02 μM towards A549 cells and also found to be 29-fold less active towards normal human embryonic kidney cells (HEK-293) with IC₅₀ of 89 ± 1.23 μM in contrast to A549 cells (Fig. 2), which indicates the selectivity of newly synthesized compounds towards cancerous cells and the SI was presented in Fig. 3.

3.2. Structure-Activity relationship (SAR)

The following conclusions have been drawn from the structure-activity relationship (SAR) analysis of the synthesized compounds based on the substitution on phenyl and imidazo[1,2-*a*]pyridine moieties:

- From the preliminary cytotoxicity screening results (Table 1), it can be noted that the presence of electron-donating (4-methoxy, 3,4-dimethoxy, 3,4,5-trimethoxy and 4-*N,N*-dimethyl) groups on the phenyl ring attached to 1,3,4-oxadiazole enhanced the bioactivity of the compounds **6c**, **6d**, **6h-j**, **6l** and **6p** as compared to the unsubstituted counterparts (**6a**, **6f** and **6m**).
- The presence of electron-withdrawing (4-chloro, 4-bromo and 2-iodo) groups on the phenyl ring linked to 1,3,4-oxadiazole were

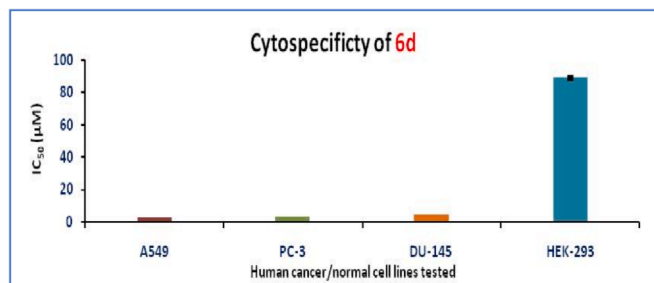


Fig. 2. Cytospecificity exhibited by compound **6d** towards human cancer cell lines tested in comparison to normal human embryonic kidney cells.

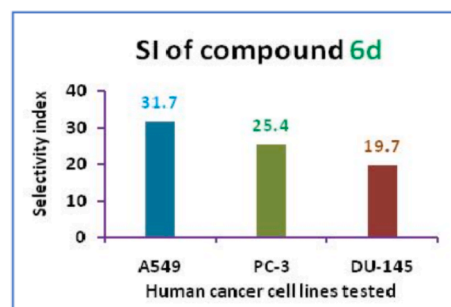


Fig. 3. Selectivity Index (SI) of lead molecule **6d**.

found to reduce the activity of the compounds (**6b**, **6e**, **6g**, **6k**, **6n** and **6o**).

- Unsubstituted imidazo[1,2-*a*]pyridines (**6d**) were relatively more active in comparison to the methyl substituted imidazo[1,2-*a*]pyridine containing compound (**6l**).

4. Flow cytometric analysis

4.1. Apoptosis detection study by annexin V/PI dual staining assay

The results from the MTT assay demonstrated that **6d** is cytotoxic in A549 cells. Annexin V-FITC/Propidium iodide dual staining assay expedites the quantification of apoptotic cell death using flow cytometry. This assay identifies the percentage of necrotic cells, late apoptotic cells, early apoptotic cells and live cells after 48 h treatment of HEK and A549 cells with **6d** compound. The apoptotic assay was performed to verify the percentage of cancer cells undergoing apoptosis upon treatment of about 2.8 μM concentration of **6d**. When A549 cells were harvested in the absence of **6d**, viable cells are ~ 83.1% and only 0.1% apoptotic (both pre and post apoptotic cells) and 0.9% necrotic cells are observed. Similarly, in HEK cell line in the absence of **6d**, viable cells are ~80.2% and only 0.2% apoptotic (both pre and post apoptotic cells) and 0.5% necrotic cells are observed. But when HEK and A549 cells were treated with 2.8 μM of **6d** compound, the percentage of viable and apoptotic cells are 18.5% and 74.5% (both pre and post apoptotic cells) respectively among HEK cells and the viable and apoptotic cells are 4.3% and 86.5% (both pre and post apoptotic cells) respectively among A549 cells. From the assay, it is evident that the **6d** compound will induce apoptosis among A549 cells much effectively compared to control HEK cells. The details are shown in Fig. 4a and quantitatively expressed as a bar graph in Fig. 4b.

4.2. Cell cycle analysis

Cells undergo spontaneous cell divisions in a systematic manner that is called the cell cycle. Most of the chemotherapeutic agents exhibit their growth inhibitory potential by the obstruction of the cell cycle at a specific checkpoint. *In vitro* cytotoxicity suggests that the compound **6d** displayed significant cytotoxicity against the A549 cell line. A cell cycle analysis study was performed to understand the role of **6d** in different phases of cell cycle, wherein untreated HEK cells were considered as a control. The distribution percentages of untreated A549 cells in sub-G1, G0/G1, S, and G2/M phases were 4.2%, 73.0%, 12.7 % and 10.1%, respectively. Upon treatment of A549 cells, with 2.8 μM of **6d**, there is a slight change in the distribution of cells in G0/G1 and a significant change in the G2/M phase compared to treated HEK cells. After treatment, the percentages of cells in sub-G1, G1, S, and G2/M phases were 1.3%, 74.5%, 6.9% and 17.1%, respectively. After the treatment of A549 cells with **6d**, the percentage of cells in G0/G1 and G2/M phase has increased from 73 to 74.5% and 10.1% to 17.1% respectively. Whereas when HEK cells were treated with 2.8 μM of **6d**, the percentages of cells in sub-G1, G1, S, and G2/M phases are 2.1%, 63.2%, 18.8% and 15.7%, respectively, compared to untreated HEK cells (sub-G1, G1, S, and G2/M

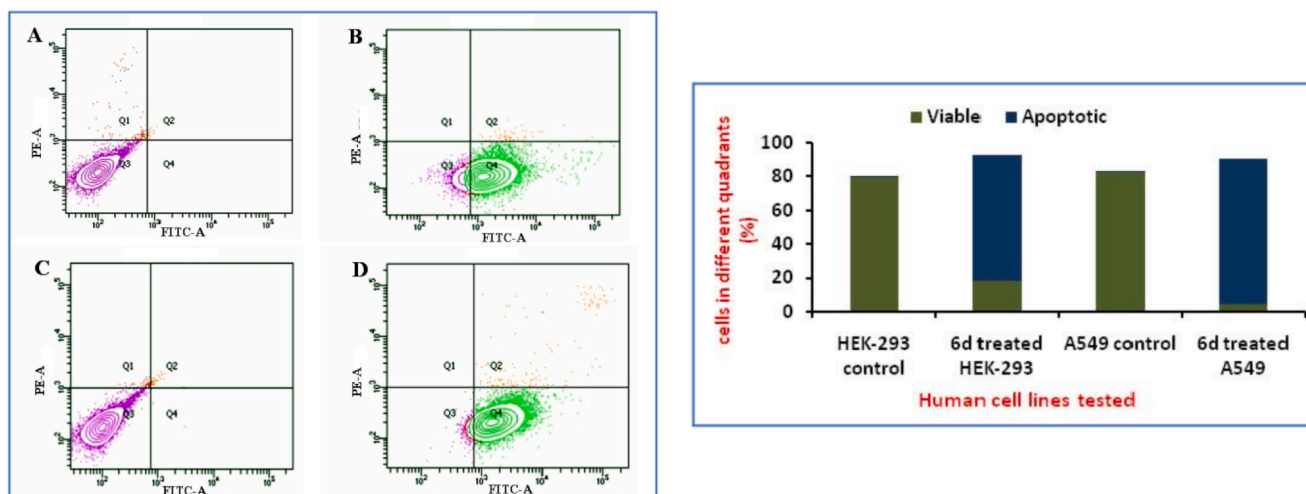


Fig. 4. (a) Annexin-V/PI dual staining assay of compound **6d** in human cancer and normal human cell lines. Flow cytometric analysis and the percentage of Annexin V-FITC/PI positive cells were represented in four quadrants. Images A and C depict the control HEK-293 and A549 cells respectively. Images B and D represent the **6d** treated HEK-293 and A549 cells respectively. (b) Bar graph quantifying the viable and apoptotic (early and late) cells.

phases were 1%, 64.1%, 18.8% and 16.1%, respectively). In HEK cells, the cell cycle did not show accumulation of cells in the G0/G1 and G2/M phase. The cell cycle and apoptosis assay indicate that compound **6d** has moderate effect on apoptosis induction and cell cycle inhibition. The details of the distribution of cells in different phases of the cell cycle are shown in Fig. 5a and quantified as bar graphs in Fig. 5b.

5. Target assays

Results from the previous experiments indicate that the compound **6d** is efficient in inducing apoptosis among cancer cells. Cell cycle reveals the ability of compound **6d** to arrest cell cycle at both G0/G1 and G2/M phase in A549 cells. Therefore to evaluate the efficiency of compound **6d** on different targets in cancer, further target based analysis (tubulin & DNA based studies) was performed.

5.1. Tubulin polymerization inhibition study

Further, to check the probable mechanism of action of these molecules in inhibition of tubulin polymerization, an enzyme based inhibitory assay along with immunohistochemistry assay was performed to examine the *in situ* effects on cellular microtubules in A549 cells.

5.1.1. Enzyme based assay

To identify the tubulin inhibitory potential of novel imidazo[1,2-*a*]pyridine-oxadiazole hybrids, the different concentrations (0.5, 1, 2, 4 and 8 μM) of compound **6d** along with 3 μM of podophyllotoxin were used for the cell-free *in vitro* tubulin polymerization assay by examining the change in fluorescence emission at 440 nm (excitation wavelength is 360 nm) for 1 h at 37 $^{\circ}\text{C}$ (Fig. 6a). The assay was performed in duplicates and it was observed that at concentrations of 0.5, 1, 2, 4 and 8 μM , there is 4.6%, 11.5%, 21.7%, 60.1% and 81.2% of inhibition of tubulin polymerization respectively, in comparison to the vehicle group (DMSO) (Fig. 6b). Remarkably, the compound **6d** exhibited noteworthy inhibition of tubulin polymerization in dose dependent mode with an IC_{50} value of $3.45 \pm 0.51 \mu\text{M}$.

5.1.2. Immunohistochemical assay

The effect of **6d** was considered in A549 cells only because in the previous experiments, the effect of **6d** was maximum on A549 cells only compared to other cells. Since the effect was high in A549 cells, they were treated with **6d** compound at half maximal inhibitory concentration for 48 h. The cells that are not treated with **6d** and podophyllotoxin

are considered positive controls. Confocal microscopic results suggested that untreated cancer cells displayed the normal distribution of microtubules, whereas cells treated with **6d** compound as well as podophyllotoxin showed the disrupted microtubule organization as shown in Fig. 7, demonstrating the inhibition of tubulin polymerization.

5.2. DNA binding studies

5.2.1. UV-Visible spectral studies

The interaction of compound **6d** with CT-DNA was studied to understand the mode of DNA interaction with the selected ligand. The compound **6d**-DNA complex UV-visible spectra displayed a prominent absorption peak at around 301 nm and 312 nm. In the present study, when equal proportions of different DNA were added to a fixed concentration of the compound, the complex absorption band displayed a continuous increase in its intensity (hyperchromicity). The **6d**-DNA complex absorption band has not shown any shift. Continuous hyperchromicity of the complex absorption band with the compound **6d** with the addition of DNA solution is an indication of very good interaction of the compound with CT-DNA. After each successive addition of CT-DNA to **6d** solution, samples were equilibrated for 5 min before measurement. The data obtained were fitted to equation (1), to obtain the dissociation constant (K_d) taking into account the total amount of 1:1 complex formed, independently of the derivative binding site(s).

$$K_d = \frac{[\text{CT} - \text{DNA}] [\text{LC/LMcompound}]}{[\text{CT} - \text{DNA.LC/LMcompound}]} \quad (1)$$

Based on the absorbance values obtained, the **6d** CT-DNA dissociation constant (K_d) was calculated using equation (1). The K_d values obtained on the interaction of **6d** with CT-DNA is 42 nM. Lower values K_d values indicate that **6d** has a better binding affinity with CT-DNA. The UV-Visible spectra profile obtained when **6d** interacts with that of CT-DNA is shown in Fig. 8.

5.2.2. Fluorescence studies

Fluorescence study is an additional important method to scrutinize the mode of binding of small molecules with the DNA and to study the electronic environment around the DNA-complex at comparatively lower concentrations. Since the complexes are fluorescent, their interaction with DNA can be monitored at low concentration with this study. **6d** compound is excited at 250 nm and the emission spectra obtained after the interaction with CT-DNA show a prominent peak at around 360 nm. When an equal quantity of DNA is added to the **6d**, the emission

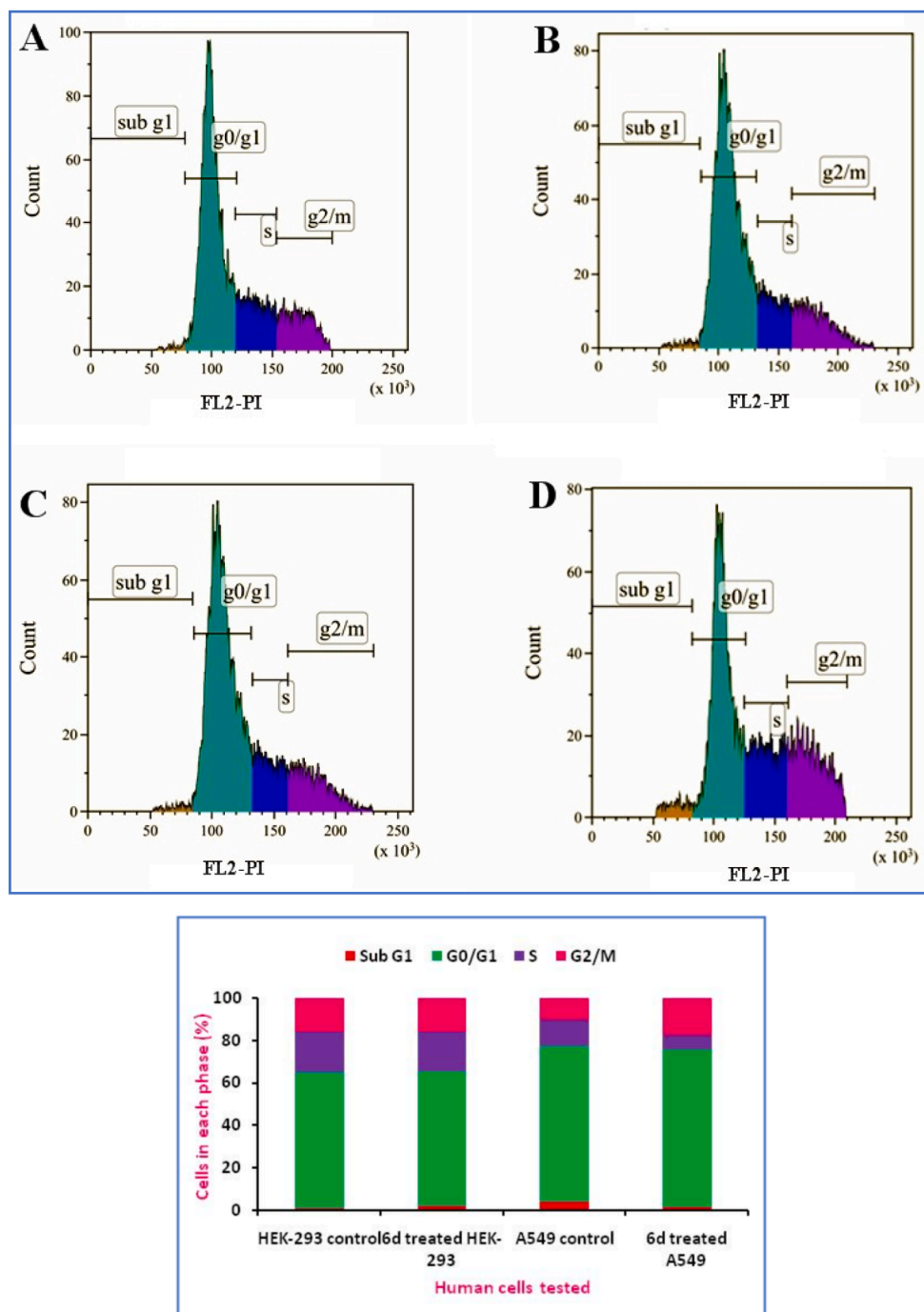


Fig. 5. (a) Flow cytometric analysis of cell cycle distribution. Dot plots were obtained on the treatment of HEK and A549 cells with 2.8 μM of compound **6d**. Image A. HEK cells before the treatment of **6d**. Image B. HEK cells after the treatment of **6d**. Image C. A549 cells before the treatment of **6d**. Image D. A549 cells after the treatment of **6d**. (b) The bar graph represents the quantification of cells at different phases of the cell cycle. The untreated controls were compared with compound **6d** treated respective cells and cell cycle arrest in human normal kidney cells (HEK-293) was compared with human lung cancer cells (A549).

peak intensity reduced gradually, indicating that the **6d** compound may be binding to the surface of DNA or binding to the groove of double helical DNA. With the increase in DNA concentration, the emission intensity gradually decreased may be due to self-stacking of the compound and binding to the DNA surface.³¹ The fluorescence spectral profile obtained on the addition of DNA to **6d** is shown in Fig. 9.

5.2.3. Circular dichroism (CD) spectroscopic studies

In spectroscopic studies like UV-visible and fluorescence studies has indicated that the compound **6d** is interacting with DNA, which may be through minor groove binding. But the effect of **6d** interaction on the

conformation of DNA can be evaluated with circular dichroism spectral studies only. To understand it better, CD spectroscopy experiments are performed. These studies will further indicate the conformational changes of double stranded CT-DNA during interaction with ligands like **6d**. CT-DNA exhibited a characteristic DNA conformation with a positive peak around 270 nm and a negative peak around 240 nm. But the CT-DNA showed positive peaks at 279 and 260 nm and negative peak at 245 nm, whereas dsDNA has shown a positive peak at 290 nm and a negative peak at around 238 nm. On addition of **6d** compound, the positive peak decreased its intensity and the negative peak intensity has reduced (Fig. 10). This indicates that on interaction with **6d**, CT-DNA

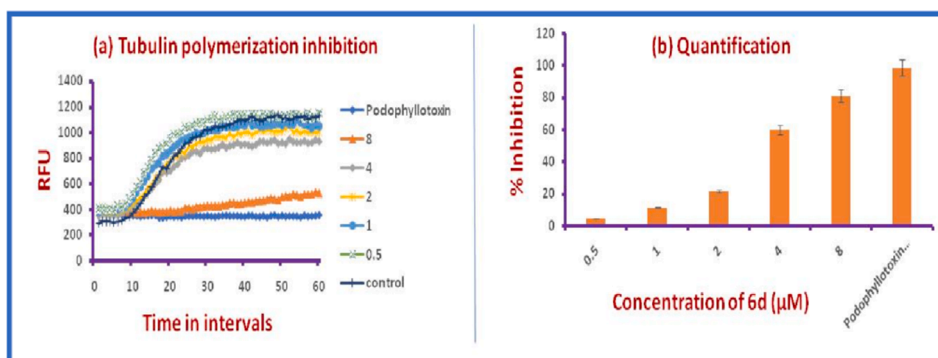


Fig. 6. (a) Effect of compound **6d** on the tubulin polymerization: tubulin polymerization was monitored by the increase in fluorescence at 360 nm (excitation) and 440 nm (emission) for 1 h at 37 °C. (b) % Dose-response inhibition of tubulin polymerization by compound **6d** at different concentrations 0.5, 1, 2, 4 and 8 µM. Podophyllotoxin was used as standard. Data expressed as mean \pm SEM (n = 3).

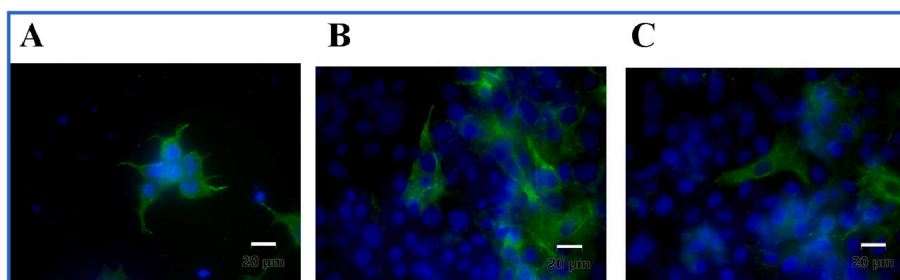


Fig. 7. A. Status of tubulin polymerization in untreated A549 cells. B. Status of tubulin polymerization in the presence of podophyllotoxin in A549 cells. C. Status of tubulin polymerization in the presence of **6d** molecule in A549 cells.

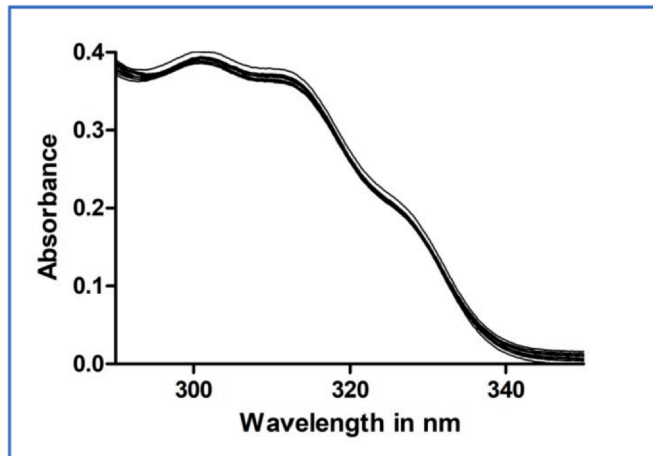


Fig. 8. UV-visible spectra of **6d** on interaction with CT-DNA. The absorption spectra exhibited slow hyperchromicity on interaction with CT-DNA. Concentration of **6d** is 10 µM and each time about 0.5 µM of CT-DNA was added.

started melting and the change in the negative peak intensity indicates that there is a change in the helix of CT-DNA.

5.2.4. Relative viscosity experiment

From the spectroscopic studies, it is seen that the potent **6d** derivative interacted well with DNA. Further, to understand the nature and mode of interaction of **6d** with double helical DNA, viscosity studies are carried out. When a molecule intercalates between the DNA, the relative viscosity increases due to the increase in the axial length, whereas, the reduction is observed with covalent DNA binding.^{32,33} Furthermore, DNA surface binding results in a slight change in the relative viscosity.³⁴

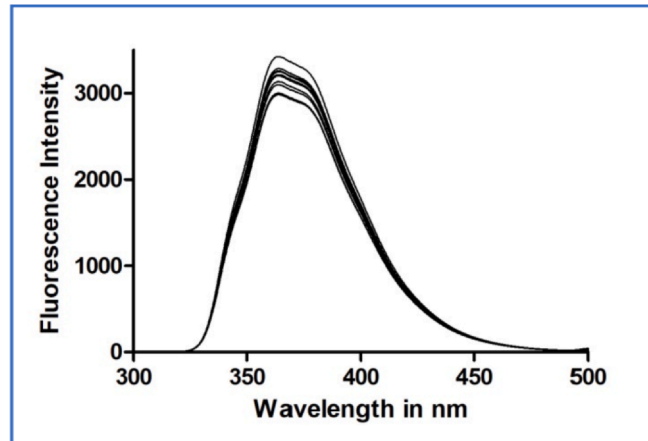


Fig. 9. Fluorescence spectra of **6d** on interaction with CT-DNA. The fluorescence spectra exhibited slow hypochromicity on interaction with CT-DNA. Concentration of **6d** is maintained at 10 µM throughout the fluorescence titration. Each time about 0.5 µM of CT-DNA was added.

As shown in Fig. 11, the interaction of **6d** with DNA resulted in a slight enhancement in viscosity. The increase in viscosity of DNA and ligand complex is moderate. The result shows that variation in DNA viscosity is between ethidium bromide (EtBr) and Hoechst 33342, but closer to Hoechst 33342 indicating that the molecules **6d** may be binding to the minor groove or to the surface of DNA. All the spectroscopic and viscosity studies results indicate that the molecule **6d** exhibited moderate interaction with DNA.

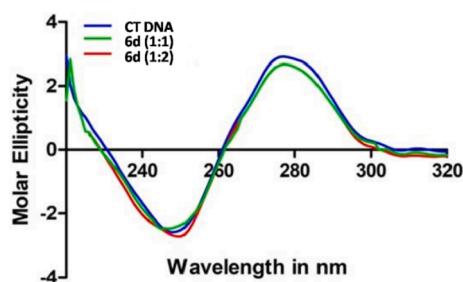


Fig. 10. CD spectra of **6d** upon interaction with CT-DNA. The spectra shown are recorded when 1:1 and 1:2 ratios CT-DNA: compound **6d** is added.

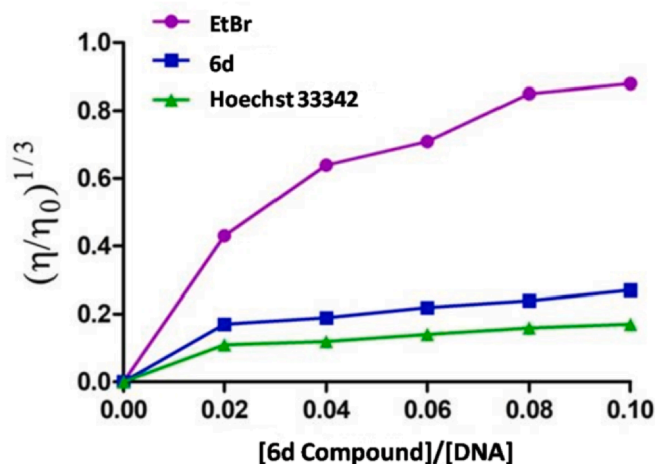


Fig. 11. Viscosity variation in CT-DNA occurred when it is allowed to interact with **6d**, EtBr and Hoechst 33342.

6. Molecular modelling studies

6.1. Molecular docking

The molecular docking study was carried out to explore the binding mode of **6d** within the active pocket of the α/β -tubulin receptor using

Schrödinger Suite release 2019–1.³⁵ The protein crystal structure of α/β -tubulin receptor was retrieved from the RCSB Protein Data Bank (PDB ID: 3E22).³⁶ The docking procedure was followed using the standard protocol implemented in Maestro and the ligand was docked against the active site of α/β -tubulin. Compound **6d** was well accommodated at the active pocket of α/β -tubulin and has shown a good number of interactions with the active site residues. Fig. 12 illustrates the predicted binding mode and the detailed protein-ligand interactions of **6d** with the active site residues of α/β -tubulin receptor. The nitrogen atom of the oxadiazole moiety of compound **6d** acts as hydrogen bond acceptor and formed two H-bond interactions with Asn249, Ala250 with a distance of 3.54 Å and 3.17 Å, respectively. The 3,4,5-trimethoxyphenyl ring of the compound **6d** established a π -cation (arene-cation) interaction with the active site residue Lys254 ($d = 3.95$ Å). Additionally, several hydrophobic interactions were observed between the compound **6d** and the active site residues, i.e. Ala250, Ala180, Val181, Tyr224, Leu248, Leu255, Met259, Val315 and Ala316. Based on the molecular docking studies, it is clear that compound **6d** well lodged in the tubulin α and β interface thereby allowing favorable interactions followed by the inhibition of tubulin polymerization.

6.2. Prime MM/GBSA binding energy calculations

MM-GBSA (Molecular mechanics generalized born surface area) approach available in the Prime module was employed to calculate the binding free energy of **6d** with protein using the OPLS3e force field. Compound **6d** energy was minimized and simulation was performed using the VSGB energy model. VSGB energy model incorporates an implicit solvation system, which is priorly optimized and performs physics-based corrections for various interactions.

From the MM-GBSA binding free energy calculations, compound **6d** has shown comparable binding energy with that of co-crystallized ligand (Table 2). The study shows that the compound **6d** has capable of binding and inhibiting tubulin enzyme.

6.3. In silico ADME/T studies

QikProp program of Schrödinger software was utilized to assess the drug-like physicochemically important descriptors and

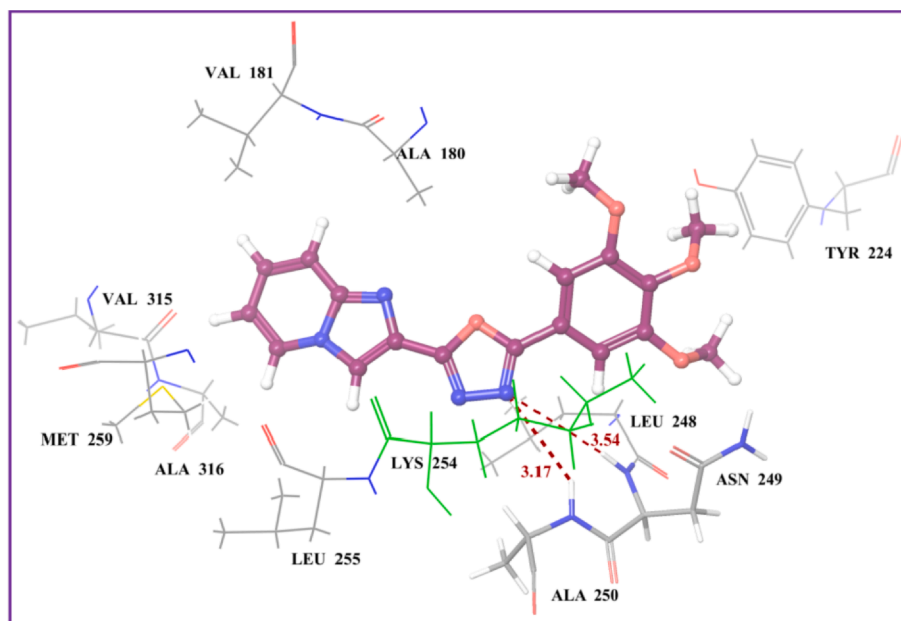


Fig. 12. Predicted docking pose of compound **6d** (purple color stick) and its ligand-protein interactions in the binding site of the α/β -tubulin receptor (PDB ID: 3E22). The red dashed lines represent hydrogen bonds. H-bond distances (in Å) between heteroatoms of ligand and amino acid residues are as follows: Asn249 (3.54), Ala250 (3.17). Green color wire indicates residue (Lys254) involved in arene-cation interaction with **6d**.

Table 2

The average binding (ΔG_{Bind}) free energy (Kcal/mol) results from MM-GBSA calculations.

S. No	^a ΔG_{Bind}	^b ΔG_{Bind} Coulomb	^c ΔG_{Bind} Covalent	^d ΔG_{Bind} H-Bond	^e ΔG_{Bind} Lipo	^f ΔG_{Bind} Solv GB	^g ΔG_{Bind} packing	^h ΔG_{Bind} vdW
6d	-73.462	-19.563	6.970	-0.400	-31.959	24.370	-1.257	-51.622
Co-crystal	-84.640	-16.229	6.757	-0.127	-52.160	28.196	0.000	-51.078

^a Free energy of binding; ^bCoulomb energy; ^cCovalent energy (internal energy); ^dHydrogen-bonding correction; ^eLipophilic energy; ^felectrostatic solvation energy; ^gPi-pi packing correction; ^hVan der Waals energy.

pharmacokinetically key properties of **6d**. Some of the computed ADME/T parameters and their recommended ranges are mentioned in Table 3. ADME/T prediction studies reveal that **6d** conforms to Lipinski's rule of five and has an appropriate logP value. Additionally, the recommended ranges of physicochemical properties were also in the acceptable range.

7. Conclusion

In conclusion, we have successfully synthesized, characterized and evaluated a series of novel imidazo[1,2-*a*]pyridine-oxadiazole hybrids and studied their anti-cancer potential. Anti-proliferative activities of the synthesized compounds were evaluated in lung cancer (A549) and prostate cancer (PC-3, DU-145) cell lines using MTT assay. Amongst the synthesized compounds, **6d** showed excellent anti-proliferative activity on all the tested cell lines, particularly in lung cancer cell lines A549 ($IC_{50} 2.8 \pm 0.02$). The cell cycle analysis disclosed that **6d** showed significant G2/M phase arrest in A549 cells. Additionally, an immunohistochemistry assay on A549 cell lines showed, compound **6d** significantly disrupted the microtubule organization. Further, target based studies demonstrated the tubulin polymerization inhibition of compound **6d** at an IC_{50} value of $3.45 \pm 0.51 \mu\text{M}$ and also exhibited effective binding with CT-DNA. The molecular modelling studies inferred that **6d** binds at the active site of α/β -tubulin with prominent binding affinity. Furthermore, we have examined physico-chemical and ADME/T properties of **6d**, which are in the acceptable range.

Table 3
ADME/T profile of **6d**.

S. No.	ADME/T Parameters	Recommended Values or Range	6d
1	Rule of five	Maximum is 4	No violation
2	PSA (van der Waals surface area of polar nitrogen and oxygen atoms and carbonyl carbon atoms)	7.0–200.0	75.245
3	SASA (Total solvent accessible surface area)	300.0–1000.0	612.224
4	Dipole Moment	1.0–12.5	9.361
5	Molecular Volume	500.0–2000.0	1077.231
6	Donor HB	0.0–6.0	0.000
7	Acceptor HB	2.0–20.0	6.250
8	QPlogKhsa (Prediction of binding to human serum albumin)	-1.5 to 1.5	-0.054
9	QPlogPo/w (Predicted octanol/water partition coefficient)	-2.0 to 6.5	3.122
10	QPpolarz (Predicted polarizability in cubic angstroms)	13.0–70.0	37.953
11	QPlogBB (Predicted brain/blood partition coefficient)	-3.0 to 1.2	-0.337
12	QPlogKp (Predicted skin permeability)	-8.0 to -1.0	-1.525
13	QPlogHERG (Predicted IC_{50} value for blockage of HERG K^+ channels.)	concern below -5	-5.741
14	QPpCaco (Predicted apparent Caco-2 cell permeability in nm/sec.)	<25 is poor, >500 great	1950.450
15	POA (Predicted human oral absorption on 0–100% scale)	>80% is high <25% is poor	100.000

8. Experimental section

8.1. Chemistry

Materials and methods: All the starting materials, chemicals and solvents were procured from commercial suppliers and used without further purification. Analytical thin layer chromatography (TLC) was performed using MERCK® pre-coated silica gel 60-F-254 (0.5 mm) aluminum plates. Visualization of spots on TLC plates was achieved by UV light. Wherever required, column chromatography was performed with silica gel (60–120 mesh). Ethyl acetate and hexane were used as eluents. Melting points were checked using Stuart digital SMP 30 melting point apparatus and were uncorrected. ¹H and ¹³C NMR spectra were recorded on Bruker NMR instrument operated at 500 and 125 MHz, respectively using tetra methyl silane (TMS) as the internal reference. Chemical shift values were given in ppm and *J* values were documented in Hertz. Spin multiplicities were explained as s (singlet), d (doublet), t (triplet), dd (doublet of doublet), q (quartet) and m (multiplet). HRMS were obtained with Agilent QTOF mass spectrometer 6540 series instrument and were performed in the ESI technique at 70 eV.

8.1.1. General procedure for the synthesis of substituted ethyl imidazo[1,2-*a*]pyridine-2-carboxylate (3)

A solution of 2-amino pyridine (1) (1 mmol) in ethanol (10 mL) was stirred at 0–5 °C. To this solution, ethylbromopyruvate/3-bromo-2-oxopropionicacidethylester (2, 1.5 mmol) was added drop-wise within 15 min. During the addition, reaction mixture turns white due to the formation of pyridinium salt. On completion of addition, the reaction mixture was stirred under reflux for 12 h. After the completion of the reaction, as monitored by TLC, the reaction mixture was cooled to room temperature. The reaction mixture was partitioned between ethyl acetate (3 × 30 mL) and water (150 mL). The organic layer was separated, dried over anhydrous Na_2SO_4 and concentrated under reduced pressure to obtain the desired imidazo[1,2-*a*]pyridine-carboxylic acid ethyl ester (3) as a light brown solid.

8.1.2. General procedure for the synthesis of substituted imidazo[1,2-*a*]pyridine-2-carbohydrazide (4)

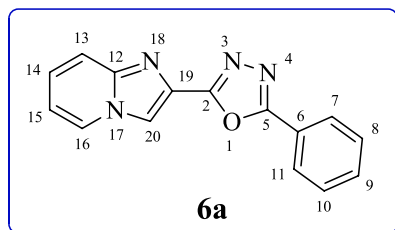
The crude imidazo[1,2-*a*]pyridine-carboxylic acid ethyl ester (3, 1 mmol) was dissolved in ethanol and hydrazine hydrate (2 mmol) was added. Then, the mixture was refluxed for about 12 h. After completion of the reaction as monitored by TLC, the reaction mixture was extracted with ethyl acetate (3 × 30 mL). The combined organic layers were washed with brine solution, dried over anhydrous Na_2SO_4 and concentrated under reduced pressure to yield imidazo[1,2-*a*]pyridine-2-carbohydrazide (4) in good yields.

8.1.3. General procedure for the synthesis of 2-(imidazo[1,2-*a*]pyridin-2-yl)-5-phenyl-1,3,4-oxadiazole (6a-p)

A solution of imidazo[1,2-*a*]pyridine-2-carbohydrazide (4, 1 mmol), substituted benzoic acid (5) (1 mmol) and POCl_3 (8 mL) was refluxed with stirring for 10–12 h. The reaction mixture was cooled and poured over crushed ice and quenched by saturated ice-cold solution of NaOH. The precipitate thus obtained was filtered washed with sodium bicarbonate. When the precipitate was not formed, the mixture was extracted

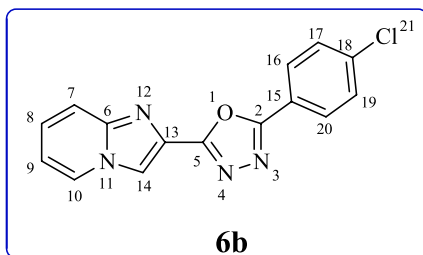
with ethyl acetate (3 × 30 mL). The combined organic layers were washed with brine solution, dried over anhydrous Na₂SO₄ and concentrated under reduced pressure to give desired product in good yields. Further compounds were purified by using column chromatography.

8.1.3.1. 2-(Imidazo[1,2-a]pyridin-2-yl)-5-phenyl-1,3,4-oxadiazole (6a)



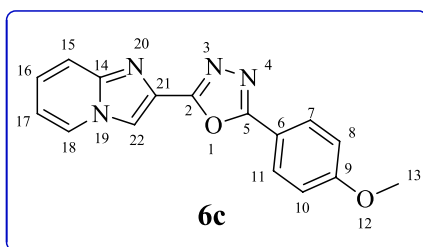
White solid, yield 96%; mp: 218–220 °C; ¹H NMR (500 MHz, DMSO-*d*₆): δ 8.81 (s, 1H), 8.67 (d, *J* = 6.8 Hz, 1H), 8.12 (dd, *J* = 7.5, 1.8 Hz, 2H), 7.73 (d, *J* = 9.1 Hz, 1H), 7.66 (dd, *J* = 10.4, 5.1 Hz, 3H), 7.45–7.40 (m, 1H), 7.07 (t, *J* = 6.6 Hz, 1H); ¹³C NMR (125 MHz, DMSO-*d*₆): δ 164.2 (C5), 161.4 (C2), 145.8 (C12), 132.5 (C9), 130.0 (C8, C10), 129.9 (C19), 128.0 (C6), 127.3 (C16), 127.1 (C7, C11), 123.9 (C14), 117.9 (C13), 115.3 (C20), 114.2 (C15); HRMS (ESI): *m/z* calcd for C₁₅H₁₁N₄O₂ 263.0933, found 263.0930 [M+H]⁺.

8.1.3.2. 2-(4-Chlorophenyl)-5-(imidazo[1,2-a]pyridin-2-yl)-1,3,4-oxadiazole (6b)



White solid, yield 88%; mp: 250–253 °C; ¹H NMR (500 MHz, DMSO-*d*₆): δ 8.81 (s, 1H), 8.66 (d, *J* = 6.8 Hz, 1H), 8.12 (d, *J* = 7.3 Hz, 2H), 7.76–7.70 (m, 3H), 7.45–7.39 (m, 1H), 7.07 (t, *J* = 6.7 Hz, 1H); ¹³C NMR (125 MHz, DMSO-*d*₆): δ 163.4 (C5), 161.5 (C2), 145.8 (C12), 137.2 (C9), 130.16 (C8, C11), 129.8 (C19), 128.9 (C7, C11), 128.1 (C6), 127.3 (C16), 122.7 (C14), 117.9 (C13), 115.4 (C20), 114.2 (C15); HRMS (ESI): *m/z* calcd for C₁₅H₁₀ClN₄O₂ 297.0543, found 297.0593 [M+H]⁺.

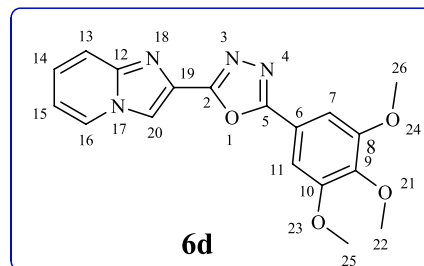
8.1.3.3. 2-(Imidazo[1,2-a]pyridin-2-yl)-5-(4-methoxyphenyl)-1,3,4-oxadiazole (6c)



Dark grey solid, yield 91%; mp: 233–235 °C; ¹H NMR (500 MHz, TriFluoro Acetic Acid (TFA)): δ 9.46 (s, 1H), 9.35 (d, *J* = 6.2 Hz, 1H), 8.71 (dd, *J* = 18.5, 8.1 Hz, 3H), 8.62 (d, *J* = 9.0 Hz, 1H), 8.20 (t, *J* = 6.5 Hz, 1H), 7.76 (d, *J* = 8.4 Hz, 2H), 4.54 (s, 3H); ¹³C NMR (125 MHz, TriFluoro Acetic Acid (TFA)): δ 168.1 (C5), 165.7 (C9), 155.2 (C2), 142.1 (C12), 138.4 (C19), 130.9 (C7, C11), 130.1 (C16), 120.1 (C14), 117.6 (C6), 116.1 (C13), 112.9 (C8, C10), 112.4 (C20), 111.6 (C15), 55.6 (C22); HRMS (ESI): *m/z* calcd for C₁₆H₁₃N₄O₂ 293.1039, found 293.1058

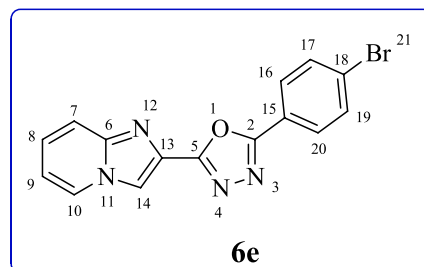
[M+H]⁺.

8.1.3.4. 2-(Imidazo[1,2-a]pyridin-2-yl)-5-(3,4,5-trimethoxyphenyl)-1,3,4-oxadiazole (6d)



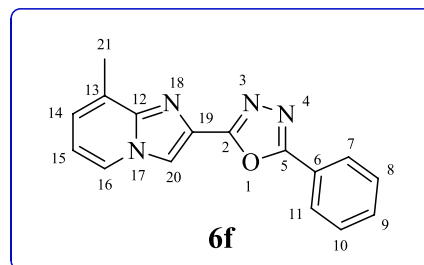
Dark grey solid, yield 93%; mp: 245–247 °C; ¹H NMR (500 MHz, TriFluoro Acetic Acid (TFA)): δ 8.98 (s, 1H), 8.87 (d, *J* = 6.7 Hz, 1H), 8.28–8.20 (m, 1H), 8.15–8.08 (m, 1H), 7.70 (t, *J* = 6.9 Hz, 1H), 7.57 (s, 2H), 4.12 (s, 3H), 4.09 (s, 6H); ¹³C NMR (125 MHz, TriFluoro Acetic Acid (TFA)): δ 167.1 (C5), 155.2 (C2), 153.7 (C8, C10), 141.8 (C12), 141.4 (C9), 137.7 (C19), 129.5 (C6), 119.4 (C16), 119.5 (C14), 117.0 (C13), 116.5 (C20), 112.2 (C15), 105.5 (C7, C11), 60.9 (C22), 55.7 (C25, C26); HRMS (ESI): *m/z* calcd for C₁₈H₁₇N₄O₄ 353.1250, found 353.1290 [M+H]⁺.

8.1.3.5. 2-(4-Bromophenyl)-5-(imidazo[1,2-a]pyridin-2-yl)-1,3,4-oxadiazole (6e)



Light grey solid, yield 82%; mp: 260–262 °C; ¹H NMR (500 MHz, TriFluoro Acetic Acid (TFA)): δ 9.42 (s, 1H), 9.31 (d, *J* = 6.7 Hz, 1H), 8.74–8.66 (m, 1H), 8.58 (d, *J* = 9.1 Hz, 1H), 8.52 (d, *J* = 8.4 Hz, 2H), 8.31 (d, *J* = 8.4 Hz, 2H), 8.16 (t, *J* = 6.9 Hz, 1H); ¹³C NMR (125 MHz, TriFluoro Acetic Acid (TFA)): δ 167.7 (C2), 155.7 (C5), 142.0 (C6), 138.3 (C13), 133.8 (C19, C17), 130.8 (C18), 130.0 (C15), 129.2 (C20, C16), 120.2 (C10), 120.1 (C8), 119.4 (C7), 117.6 (C14), 112.8 (C9); HRMS (ESI): *m/z* calcd for C₁₅H₁₀BrN₄O 341.0038, found 341.0124 [M+H]⁺.

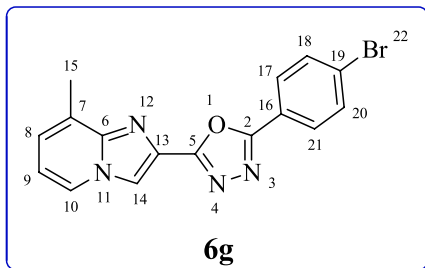
8.1.3.6. 2-(8-Methylimidazo[1,2-a]pyridin-2-yl)-5-phenyl-1,3,4-oxadiazole (6f)



White solid, yield 89%; mp: 226–232 °C; ¹H NMR (500 MHz, DMSO-*d*₆): δ 8.80 (s, 1H), 8.51 (d, *J* = 6.6 Hz, 1H), 8.12 (d, *J* = 6.1 Hz, 2H), 7.66 (d, *J* = 6.3 Hz, 3H), 7.22 (d, *J* = 6.6 Hz, 1H), 6.97 (t, *J* = 6.7 Hz, 1H), 2.58 (s, 3H); ¹³C NMR (125 MHz, DMSO-*d*₆): δ 164.1 (C5), 161.5 (C2), 146.4 (C12), 132.5 (C9), 130.0 (C8, C10), 129.5 (C19), 127.5 (C14), 127.1 (C7, C11), 125.7 (C6), 125.5 (C13), 123.8 (C16),

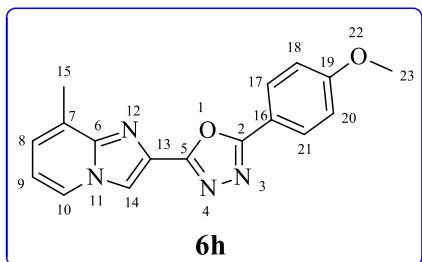
115.8 (C20), 114.2 (C15), 17.0 (C21); HRMS (ESI): m/z calcd for $C_{16}H_{13}N_4O$ 277.1108, found 277.1108 $[M+H]^+$.

8.1.3.7. 2-(4-Bromophenyl)-5-(8-methylimidazo[1,2-a]pyridin-2-yl)-1,3,4-oxadiazole (**6g**)



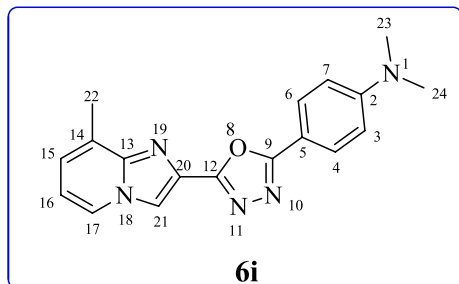
Light grey solid, yield 76%; mp: 242–243.5 °C; 1H NMR (500 MHz, DMSO- d_6): δ 8.80 (s, 1H), 8.50 (t, $J = 6.6$ Hz, 1H), 8.05 (d, $J = 8.5$ Hz, 2H), 7.87 (d, $J = 8.5$ Hz, 2H), 7.22 (d, $J = 6.8$ Hz, 1H), 6.97 (t, $J = 6.8$ Hz, 1H), 2.57 (s, 3H); ^{13}C NMR (125 MHz, DMSO- d_6): δ 163.5 (C2), 161.6 (C5), 146.4 (C6), 133.1 (C18, C20), 129.3 (C13), 129.0 (C17, C21), 127.5 (C8), 126.1 (C19), 125.7 (C7), 125.6 (C16), 123.1 (C10), 116.0 (C14), 114.2 (C9), 17.1 (C15); HRMS (ESI): m/z calcd for $C_{16}H_{14}BrN_4O$ 357.0335, found 357.0177 $[M+3H]^+$.

8.1.3.8. 2-(4-Methoxyphenyl)-5-(8-methylimidazo[1,2-a]pyridin-2-yl)-1,3,4-oxadiazole (**6h**)



Dark grey solid, yield 84%; mp: 175–178 °C; 1H NMR (500 MHz, DMSO- d_6): δ 8.76 (s, 1H), 8.50 (d, $J = 5.7$ Hz, 1H), 8.05 (d, $J = 7.8$ Hz, 2H), 7.20 (d, $J = 7.8$ Hz, 3H), 6.96 (s, 1H), 3.89 (s, 3H), 2.57 (s, 3H); ^{13}C NMR (125 MHz, DMSO- d_6): δ 164.1 (C2), 162.6 (C10), 161.0 (C5), 146.3 (C6), 129.6 (C13), 129.0 (C17, C21), 127.5 (C8), 125.7 (C7), 125.5 (C10), 116.1 (C16), 115.6 (C14), 115.4 (C18, C20), 114.1 (C9), 56.0 (C23), 17.0 (C15); HRMS (ESI): m/z calcd for $C_{17}H_{15}N_4O_2$ 307.1195, found 307.1211 $[M+H]^+$.

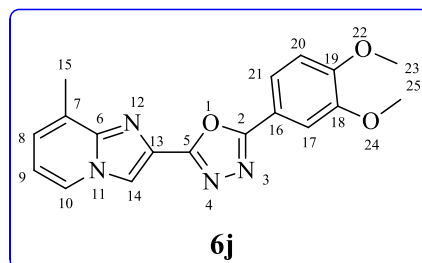
8.1.3.9. *N,N*-Dimethyl-4-(5-(8-methylimidazo[1,2-a]pyridin-2-yl)-1,3,4-oxadiazol-2-yl)aniline (**6i**)



Dark grey solid, yield 78%; mp: 247–250 °C; 1H NMR (500 MHz, TriFluro Acetic Acid (TFA)): δ 8.94 (s, 1H), 8.63 (d, $J = 6.6$ Hz, 1H), 8.47 (d, $J = 8.5$ Hz, 2H), 7.95 (t, $J = 8.6$ Hz, 3H), 7.55 (t, $J = 7.0$ Hz, 1H), 3.51 (s, 6H), 2.83 (s, 3H); ^{13}C NMR (125 MHz, TriFluro Acetic Acid (TFA)): δ 165.2 (C9), 156.1 (C12), 145.7 (C2), 141.9 (C13), 137.1 (C20), 130.5

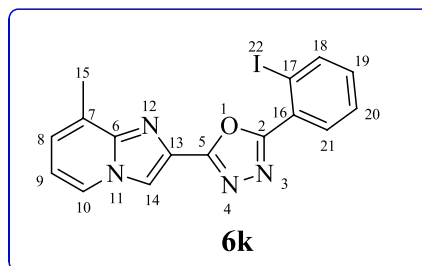
(C6, C4), 127.1 (C15), 124.4 (C14), 124.1 (C17), 121.8 (C3, C7), 119.7 (C5), 119.3 (C21), 118.1 (C16), 47.2 (C23, C24), 14.5 (C22); HRMS (ESI): m/z calcd for $C_{18}H_{18}N_5O$ 320.1511, found 320.1530 $[M+H]^+$.

8.1.3.10. 2-(3,4-Dimethoxyphenyl)-5-(8-methylimidazo[1,2-a]pyridin-2-yl)-1,3,4-oxadiazole (**6j**)



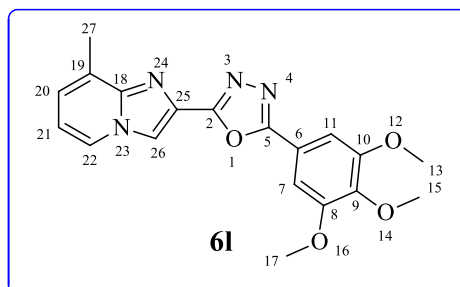
White solid, yield 90%; mp: 257–258 °C; 1H NMR (500 MHz, TriFluro Acetic Acid (TFA)): δ 8.90 (s, 1H), 8.64 (d, $J = 6.3$ Hz, 1H), 7.94 (t, $J = 13.9$ Hz, 1H), 7.87 (d, $J = 8.3$ Hz, 1H), 7.72 (s, 1H), 7.54 (t, $J = 6.8$ Hz, 1H), 7.18 (t, $J = 9.9$ Hz, 1H), 4.03 (d, $J = 8.9$ Hz, 6H), 2.82 (s, 3H); ^{13}C NMR (125 MHz, TriFluro Acetic Acid (TFA)): δ 167.3 (C2), 154.9 (C5), 154.2 (C19), 149.1 (C18), 141.8 (C6), 137.0 (C13), 127.0 (C8), 124.3 (C7), 123.4 (C10), 119.6 (C21), 119.3 (C16), 112.5 (C14), 111.8 (C9, C20), 110.1 (C17), 55.5 (C25), 55.2 (C23), 14.4 (C15); HRMS (ESI): m/z calcd for $C_{18}H_{17}N_4O_3$ 337.1301, found 337.1314 $[M+H]^+$.

8.1.3.11. 2-(2-Iodophenyl)-5-(8-methylimidazo[1,2-a]pyridin-2-yl)-1,3,4-oxadiazole (**6k**)



White solid, yield 85%; mp: 214–216 °C; 1H NMR (500 MHz, DMSO- d_6): δ 8.80 (s, 1H), 8.51 (d, $J = 6.8$ Hz, 1H), 8.17 (dd, $J = 8.0, 0.8$ Hz, 1H), 7.91 (dd, $J = 7.7, 1.5$ Hz, 1H), 7.66 (td, $J = 7.6, 1.1$ Hz, 1H), 7.41 (td, $J = 7.7, 1.6$ Hz, 1H), 7.24–7.21 (m, 1H), 6.98 (t, $J = 6.8$ Hz, 1H), 2.56 (s, 3H); ^{13}C NMR (125 MHz, DMSO- d_6): δ 164.0 (C2), 161.7 (C5), 146.4 (C6), 141.1 (C18), 133.6 (C13), 132.0 (C19), 129.4 (C21), 129.3 (C20), 129.1 (C8), 127.5 (C7), 125.7 (C10), 125.6 (C16), 116.0 (C9), 114.2 (C14), 96.6 (C17), 17.0 (C15); HRMS (ESI): m/z calcd for $C_{16}H_{12}IN_4O$ 403.0053, found 403.0081 $[M+H]^+$.

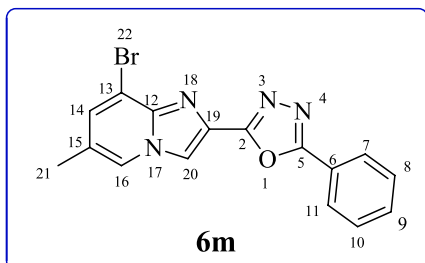
8.1.3.12. 2-(8-Methylimidazo[1,2-a]pyridin-2-yl)-5-(3,4,5-trimethoxyphenyl)-1,3,4-oxadiazole (**6l**)



White solid, yield 79%; mp: 216–218 °C; 1H NMR (500 MHz,

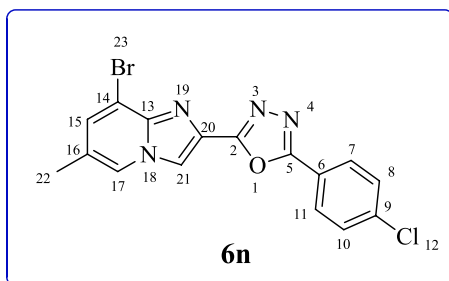
TriFluro Acetic Acid (TFA): δ 8.95 (s, 1H), 8.69 (d, $J = 5.9$ Hz, 1H), 7.99 (d, $J = 7.0$ Hz, 1H), 7.62–7.51 (m, 3H), 4.10 (d, $J = 2.2$ Hz, 3H), 4.07 (s, 6H), 2.86 (s, 3H); ^{13}C NMR (125 MHz, CDCl_3): δ 165.2 (C5), 159.5 (C2), 153.7 (C8, C10), 145.5 (C18), 145.4 (C9), 141.3 (C25), 128.1 (C20), 127.2 (C19), 124.4 (C22), 118.6 (C6), 115.2 (C26), 114.4 (C21), 104.9 (C7, C11), 61.0 (C15), 56.7 (C13, C17), 17.5 (C27); HRMS (ESI): m/z calcd for $\text{C}_{19}\text{H}_{19}\text{N}_4\text{O}_4$ 367.1406, found 367.1412 $[\text{M}+\text{H}]^+$.

8.1.3.13. 2-(8-Bromo-6-methylimidazo[1,2-a]pyridin-2-yl)-5-phenyl-1,3,4-oxadiazole (6m)



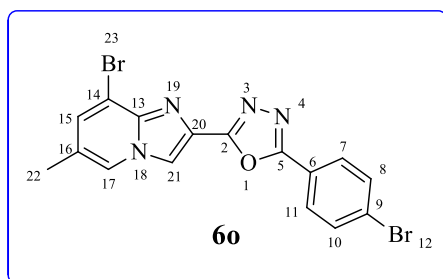
Light grey solid, yield 87%; mp: 231–232 °C; ^1H NMR (500 MHz, $\text{DMSO}-d_6$): δ 8.83 (s, 1H), 8.48 (s, 1H), 8.12 (d, $J = 6.3$ Hz, 2H), 7.75–7.57 (m, 4H), 2.32 (s, 3H); ^{13}C NMR (125 MHz, $\text{DMSO}-d_6$): δ 164.2 (C5), 161.0 (C2), 142.8 (C12), 132.6 (C14), 132.5 (C9), 130.0 (C19), 130.0 (C8, C10), 127.2 (C7, C11), 125.0 (C6), 124.1 (C15), 123.7 (C16), 116.9 (C20), 110.3 (C13), 17.7 (C21); HRMS (ESI): m/z calcd for $\text{C}_{16}\text{H}_{12}\text{BrN}_4\text{O}$ 355.0194, found 355.0196 $[\text{M}+\text{H}]^+$.

8.1.3.14. 2-(8-Bromo-6-methylimidazo[1,2-a]pyridin-2-yl)-5-(4-chlorophenyl)-1,3,4-oxadiazole (6n)



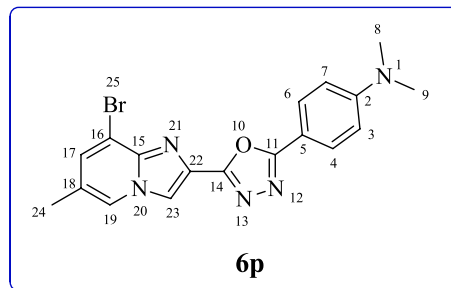
Light grey solid, yield 83%; mp: 253–255 °C; ^1H NMR (500 MHz, TriFluro Acetic Acid (TFA)): δ 9.70 (s, 1H), 9.37 (s, 1H), 9.04 (s, 1H), 8.89 (d, $J = 8.5$ Hz, 2H), 8.43 (d, $J = 8.4$ Hz, 2H), 3.37 (s, 3H); ^{13}C NMR (125 MHz, TriFluro Acetic Acid (TFA)): δ 167.9 (C5), 155.8 (C2), 143.5 (C13), 143.0 (C9), 140.4 (C15), 133.3 (C20), 131.1 (C8, C10), 129.7 (C7, C11), 127.0 (C6), 121.1 (C16), 119.2 (C17), 118.9 (C21), 105.7 (C14), 17.2 (C22); HRMS (ESI): m/z calcd for $\text{C}_{16}\text{H}_{13}\text{BrClN}_4\text{O}$ 390.9961, found 390.9832 $[\text{M}+3\text{H}]^+$.

8.1.3.15. 2-(8-Bromo-6-methylimidazo[1,2-a]pyridin-2-yl)-5-(4-bromophenyl)-1,3,4-oxadiazole (6o)



Light grey solid, yield 80%; mp: 258–260 °C; ^1H NMR (500 MHz, TriFluro Acetic Acid (TFA)): δ 9.83 (s, 1H), 9.51 (s, 1H), 9.19 (s, 1H), 8.95 (d, $J = 8.3$ Hz, 2H), 8.75 (d, $J = 8.3$ Hz, 2H), 3.52 (s, 3H); ^{13}C NMR (125 MHz, TriFluro Acetic Acid (TFA)): δ 168.2 (C5), 156.0 (C2), 143.5 (C13), 140.5 (C15), 134.2 (C20), 133.4 (C8, C10), 131.2 (C9), 129.6 (C7, C11), 127.0 (C6), 121.2 (C16, C17), 119.8 (C21), 105.8 (C14), 17.2 (C22); HRMS (ESI): m/z calcd for $\text{C}_{16}\text{H}_{13}\text{Br}_2\text{N}_4\text{O}$ 434.9456, found 434.9298 $[\text{M}+3\text{H}]^+$.

8.1.3.16. 4-(5-(8-Bromo-6-methylimidazo[1,2-a]pyridin-2-yl)-1,3,4-oxadiazol-2-yl)-N,N-dimethylaniline (6p)



White solid, yield 76%; mp: 255–259 °C; ^1H NMR (500 MHz, TriFluro Acetic Acid (TFA)): δ 9.01 (s, 1H), 8.61 (s, 1H), 8.48 (s, 2H), 8.24 (s, 1H), 7.95 (t, $J = 13.3$ Hz, 2H), 3.52 (s, 6H), 2.58 (s, 3H); ^{13}C NMR (125 MHz, TriFluro Acetic Acid (TFA)): δ 165.2 (C11), 155.7 (C14), 145.7 (C2), 142.6 (C15), 139.6 (C17), 132.3 (C22), 130.6 (C4, C6), 126.2 (C18), 124.1 (C19), 121.9 (C3, C7), 120.0 (C5), 118.7 (C23), 104.8 (C16), 47.2 (C8, C9), 16.2 (C24); HRMS (ESI): m/z calcd for $\text{C}_{18}\text{H}_{19}\text{BrN}_5\text{O}$ 400.0773, found 400.0689 $[\text{M}+3\text{H}]^+$.

8.2. Biological evaluation

8.2.1. Cell culture

Human cancer cell lines such as lung cancer (A549), prostate cancer (PC-3, DU-145) and normal human embryonic kidney (HEK-293) were obtained from National Centre for Cell Science, Pune, India. Cells were maintained in appropriate media supplemented with 10% fetal bovine serum (FBS) stabilized with 1% antibiotic-antimycotic solution (Sigma Aldrich) in the incubator at 37 °C. When the cells reached up to 80–90% of confluency, sub-culturing was performed using a 0.25% trypsin/1 mM EDTA solution for further passage.

8.2.2. MTT assay

The cytotoxicity of all newly synthesized compounds was determined by using MTT assay, where, MTT (3-(4,5-dimethylthiazol-2-yl)-2,5-diphenyl tetrazolium bromide) is a dye that converts into insoluble formazan by mitochondrial succinate dehydrogenase enzyme. In brief, cells were seeded in 96-well plates at a density of 1000–4000 cells per well in 100 μL of complete medium and allowed to grow overnight. Further, the media was replaced with fresh media and cells were treated with various concentrations of the compounds for a period of 48 h. After incubation, the media was aspirated and 100 μL of MTT (0.5 mg/mL) was added and incubated at 37 °C for 4 h. After that, MTT reagent was aspirated and the formazan crystals formed were dissolved in DMSO (200 μL) for 20 min at 37 °C. Finally, the formed formazan was measured by using a spectrophotometric microtiter plate reader at 570 nm wavelength.

8.2.3. Flow cytometric analysis

8.2.3.1. Apoptosis detection study by Annexin V/PI dual staining assay.

This assay was performed by the method given by Rieger *et al.* with slight modifications.³⁷ Briefly, 1×10^5 A549 and HEK cells were seeded in a 12-well plate and treated with 2.8 μM 6d compound for 48 h. The

collected cells were washed twice with ice-cold PBS, then incubated with 200 μL of $1 \times$ binding buffer containing 1 μL propidium iodide (PI) for 15 min at room temperature in the dark. After incubation, cells were analyzed for apoptosis using a flow cytometer (BD FACSVerser™, USA). Apoptosis and necrosis were analyzed with quadrant statistics on propidium iodide-negative cells, fluorescein positive cells, and propidium iodide (PI)-positive cells, respectively.

8.2.3.2. Cell cycle assay. To validate the results obtained from the MTT assay as well as to understand the effect of **6d** compound on cell cycle progression, cell cycle analysis was performed. Flow cytometry experiments were performed according to the reported protocol.³⁸ A549 and HEK cells were incubated with 2.8 μM of **6d** compound for 48 h. Untreated A549 and HEK cells were used as a control. Untreated and treated cells were harvested, washed with phosphate-buffered saline (PBS), fixed in ice-cold 70% alcohol, and stained with propidium iodide (PI) (Sigma-Aldrich). The cell cycle assay was performed using a Becton Dickinson FACSCalibur flow cytometer.

8.2.4. Target based assays

8.2.4.1. Tubulin polymerization assay

8.2.4.1.1. Enzyme based assay. Tubulin polymerization kit was procured from Cytoskeleton, Inc. (BK011). To study the effect of compound **6d**, fluorescence based *in vitro* tubulin polymerization assay was performed following the manufacturer's protocol. The reaction mixture having porcine brain tissue (2 mg/mL) in 80 mM PIPES at pH 6.9, 2.0 mM MgCl_2 , 0.5 mM EGTA, 1.0 mM GTP and glycerol in the presence and absence of test compound **6d** (final concentration of 10 μM) was prepared and added to each well of 96-well plate. Tubulin polymerization was followed by a time dependent increase in fluorescence due to the insertion of a fluorescence reporter into microtubules as polymerization takes place. Spectramax M4 Multi mode Micro plate Detection System was used to measure Fluorescence emission at 440 nm (excitation wavelength is 360 nm). Podophyllotoxin was used as positive control in the assay at 3 μM final concentration. The IC_{50} value was calculated from the drug concentration required for inhibiting 50% of tubulin assembly compared to control.

8.2.4.1.2. Immunohistochemistry assay. A549 cells were seeded on glass cover slips and incubated for 48 h in the presence or absence of **6d** compound and podophyllotoxin at 2 μM concentration. Podophyllotoxin was reported to show tubulin polymerization inhibition.³⁹ After treatment, the cover slips were fixed with a paraformaldehyde solution (4% in $1 \times$ PBS) for 20 min at room temperature. Cell permeabilization was achieved by administration of a Triton X-100 solution (0.2% in $1 \times$ PBS) for 5 min. The cover slips were left in 100% MeOH overnight at 4 °C. Subsequently, the cover slips were blocked with a 1% bovine serum albumin (BSA) solution for 60 min and then incubated with α -tubulin antibody (1:1000) at room temperature for 2 h. The slides were washed three times for 5 min each with PBST. Next, the cover slips were incubated with FITC conjugated anti-mouse secondary antibody (Cell signaling technology) for 1 h and then washed three times with PBST solution. Finally, the cells were observed under a confocal microscope, and the pictures were analyzed for the integrity of the microtubule network.

8.2.4.2. DNA binding studies

8.2.4.2.1. UV-Vis spectroscopic studies. UV-visible spectroscopy titrations were performed using ABI Lambda 40 UV-Vis spectrophotometer (Foster City, USA) at 25 °C using a 1 cm path length quartz cuvette. Stock solutions of 1 mM of CT-DNA (calf thymus DNA, which can form perfect double stranded DNA structure) were prepared in 100 mM Tris-HCl (pH 7.0). 1 mM stock solution of the synthesized **6d** compound was prepared by dissolving them in 1:1 DMSO: Milli Q water. UV-visible absorption titrations are performed by adding 10 μM CT-DNA solution in

100 mM Tris-HCl (pH 7.0) each time to the quartz cuvette containing about 10 μM of **6d** compound solution. Each time about 0.5 μM of CT-DNA was added to cuvette containing fixed concentration of compound **6d**. Titrations were carried out until the complex absorption band remained at a fixed wavelength upon five successive additions of CT-DNA. UV-vis spectra were recorded from 200 to 400 nm range.

8.2.4.2.2. Fluorescence titration studies. Fluorescence emission spectra were measured at 25 °C using a Hitachi F7000 spectrofluorimeter (Maryland, USA) using a 1 cm path length quartz cuvette. Throughout the fluorescence experiment, the concentration of the **6d** compound was kept constant (10 μM) and titrated with the addition of equal quantities of CT-DNA. Fluorescence spectra were recorded after each addition of CT-DNA to the compound containing fluorescent cuvette. Each time about 0.5 μM of CT-DNA was added to cuvette containing fixed concentration of compound **6d**. After each experiment, the quartz cuvettes were thoroughly washed with distilled water and dilute nitric acid (approximately 0.1 N, nitric acid) to remove traces of compound binding to the walls of the quartz cuvette. **6d** compound was excited at 250 nm, and emission spectra for each titration were collected in the range from 300 to 500 nm and the emission peak was monitored at 360 nm. Each spectrum was recorded three times and an average of three scans was taken.

8.2.4.2.3. Circular dichroism studies. Circular dichroism experiments were carried out using JASCO 815CD spectropolarimeter (Jasco, Tokyo, Japan). CD spectrum was recorded from 220 to 320 nm to find the conformational changes in CT-DNA after DNA-compound interaction. For CD experiments, 10×10^{-6} M of CT-DNA was used. For characterizing compound-CT-DNA interaction, CD spectra were recorded in 1:0, 1:1 and 1:2 M ratio of CT-DNA: **6d** compound. CD titrations were performed in 100 mM Tris-HCl (pH 7.0) at 25 °C. Each CD spectrum was recorded thrice and the average of three scans was considered.

8.2.4.2.4. Relative viscosity studies. Viscosity experiments were conducted using an Ostwald viscometer immersed in a water bath and maintained at 25 °C. Viscosity experiments were performed for **6d** compound (15 μM), after mixing them with CT-DNA solution (150 μM). Before mixing CT-DNA and **6d** compound, viscosity measurements were performed with CT-DNA alone. EtBr and Hoechst 33342 complex with CT-DNA were considered as control. The DNA solution was prepared in 100 mM Tris-HCl (pH 7.0). The graph was drawn by plotting $(\eta/\eta_0)^{1/3}$ versus compound/CT-DNA, where η is the viscosity of CT-DNA in the presence of **6d** compound and η_0 is the viscosity of CT-DNA alone. Viscosity values were calculated according to the protocol mentioned by Tan *et al.*⁴⁰

8.3. Molecular modelling

The tubulin crystal structure has been taken from the Protein Data Bank (PDB ID: 3E22). The protein preparation tool was used for the preparation of the tubulin protein. The grid is generated by picking the active site where the co-crystal is located and grid box of $10 \times 10 \times 10 \text{ \AA}$ (Schrödinger 2019–1). By using 2D sketcher the potent hybrid **6d** was sketched and energy minimized, ligand preparation was performed for the generation of different conformers (Schrödinger 2019–1). The various conformers thus obtained were subjected to molecular docking with SP Glide (Schrödinger 2019–1). The poses generated were assessed and the best one was reported.

Declaration of Competing Interest

The authors declare that they have no known competing financial interests or personal relationships that could have appeared to influence the work reported in this paper.

Acknowledgments

The authors are thankful to Department of Pharmaceuticals (DoP),

Ministry of Chemicals & Fertilizers, Govt. of India, New Delhi, for the award of NIPER fellowship.

Appendix A. Supplementary material

Supplementary data to this article can be found online at <https://doi.org/10.1016/j.bmc.2021.116277>.

References

- Siegel RL, Miller KD, Jemal A. Cancer statistics, 2020. *CA-Cancer J Clin.* 2020;70:7–30.
- Ma X, Yu H. Global burden of cancer. *Yale J Biol Med.* 2006;79:85–94.
- Nagai H, Kim YH. Cancer prevention from the perspective of global cancer burden patterns. *J Thorac Dis.* 2017;9:448–451.
- Arruibo M, Vilaboa N, Sáez-Gutiérrez B, et al. Assessment of the evolution of cancer treatment therapies. *Cancers.* 2011;3:3279–3330.
- Parker AL, Kavallaris M, McCarroll JA. Microtubules and their role in cellular stress in cancer. *Front Oncol.* 2014;4:153.
- Parker AL, Teo WS, McCarroll JA, Kavallaris M. An emerging role for tubulin isotypes in modulating cancer biology and chemotherapy resistance. *Int J Mol Sci.* 2017;18:1434.
- (a) Nekkanti S, Tokala R, Shankaraiah N. Targeting DNA minor groove by hybrid molecules as anticancer agents. *Curr Med Chem.* 2017;24:2887–2907; (b) Thomas E, Gopalakrishnan V, Hegde M, et al. A novel resveratrol based tubulin inhibitor induces mitotic arrest and activates apoptosis in cancer cells. *Sci Rep.* 2016;6:34653.
- Cesare ED, Verrico A, Miele A, et al. Mitotic cell death induction by targeting the mitotic spindle with tubulin-inhibitory indole derivative molecules. *Oncotarget.* 2017;8:19738–19759.
- Bagdi AK, Santra S, Monir K, Hajra A. Synthesis of imidazo[1,2-a]pyridines: a decade update. *Chem Commun.* 2015;51:1555–1575.
- Hosseini H, Bayat M. An efficient synthesis of new imidazo[1,2-a]pyridine-6-carbohydrazide and pyrido[1,2-a]pyrimidine-7-carbohydrazide derivatives via a five-component cascade reaction. *RSC Adv.* 2019;9:7218–7227.
- Gangireddy MR, Mantipally M, Gundla R, Badavath VN, Paidikondala K, Yamala A. Design and synthesis of piperazine-linked imidazo[1,2-a]pyridine derivatives as potent anticancer agents. *ChemistrySelect.* 2019;4:13622–13629.
- Liu T, Peng X, Ma Y, et al. Discovery of a new series of imidazo[1,2-a]pyridine compounds as selective c-Met inhibitors. *Acta Pharmacol Sin.* 2016;37:698–707.
- Goel R, Luxami V, Paul K. Imidazo[1,2-a]pyridines: Promising drug candidate for antitumor therapy. *Curr Top Med Chem.* 2016;16:3590–3616.
- Baviskar AT, Madaan C, Preet R, et al. N-fused imidazoles as novel anticancer agents that inhibit catalytic activity of topoisomerase II α and induce apoptosis in G1/S phase. *J Med Chem.* 2011;54:5013–5030.
- Sanghai N, Jain V, Preet R, et al. Combretastatin A-4 inspired novel 2-Aryl-3-arylamino-imidazopyridines/pyrazines as tubulin polymerization inhibitors, antimitotic and anticancer Agents. *Med Chem Commun.* 2014;5:766–782.
- An W, Wang W, Yu T, et al. Discovery of novel 2-phenyl-imidazo[1,2-a]pyridine analogues targeting tubulin polymerization as antiproliferative agents. *Eur J Med Chem.* 2016;112:367–372.
- Ramya PVS, Guntuku L, Angapelly S, et al. Synthesis and biological evaluation of curcumin inspired imidazo[1,2-a]pyridine analogues as tubulin polymerization inhibitors. *Eur J Med Chem.* 2018;143:216–231.
- Nayak SG, Poojary B. A Review on the preparation of 1,3,4-oxadiazoles from the dehydration of hydrazines and study of their biological roles. *Chem Afr.* 2019;2:551–571.
- Khalilullah H, Ahsan MJ, Hedaitullah M, Khan S, Ahmed B. 1,3,4-Oxadiazole: a biologically active scaffold. *Mini Rev Med Chem.* 2012;12:789–801.
- Asif M, Abida A. Mini review on biological potential of 1,3,4-oxadiazole derivatives. *Int J Pharm Chem Anal.* 2018;5:179–187.
- Bajaj S, Roy PP, Singh J. 1,3,4-Oxadiazoles as telomerase inhibitor: potential anticancer agents. *Anticancer Agents Med Chem.* 2017;17:1869–1883.
- Vaidya A, Pathak D, Shah K. 1,3,4-Oxadiazole and its derivatives: a review on recent progress in anticancer activities. *Chem Biol Drug Des.* 2020. <https://doi.org/10.1111/cbdd.13795>.
- Kamal A, Srikanth PS, Vishnuvardhan MVPS, et al. Combretastatin linked 1,3,4-oxadiazole conjugates as a potent tubulin polymerization inhibitors. *Bioorg Chem.* 2016;65:126–136.
- Kamal A, Srikanth YVV, Shaik TB, et al. 2-Anilino nicotinyllinked 1,3,4-oxadiazole derivatives: synthesis, antitumour activity and inhibition of tubulin polymerization. *Med Chem Commun.* 2011;2:819–823.
- (a) Shankaraiah N, Nekkanti S, Ommi O, Soukya PSL. Diverse targeted approaches to battle multidrug resistance in cancer. *Curr Med Chem.* 2019;26:7059–7080; (b) Meunier B. Hybrid molecules with a dual mode of action: dream or reality? *Acc Chem Res.* 2008;41:69–77; (c) Zang L, Kondengaden SM, Zhang Q, et al. Structure based design, synthesis and activity studies of small hybrid molecules as HDAC and G9a dual inhibitors. *Oncotarget.* 2017;8:63187–63207.
- Guggilapu SD, Lalita G, Reddy TS, et al. Synthesis of thiazole linked indolyl-3-glyoxylamide derivatives as tubulin polymerization inhibitors. *Eur J Med Chem.* 2017;138:83–95.
- (a) Sigalapalli DK, Pooladanda V, Singh P, et al. Discovery of certain benzyl/phenethylthiazolidinone-indole hybrids as potential anti-proliferative agents: synthesis, molecular modeling and tubulin polymerization inhibition study. *Bioorg Chem.* 2019;92:1031883; (b) Sana S, Tokala R, Bajaj DM, et al. Design and synthesis of substituted dihydropyrimidinone derivatives as cytotoxic and tubulin polymerization inhibitors. *Bioorg Chem.* 2019;93, 103317; (c) Jadala C, Sathish M, Anchi P, et al. Synthesis of combretastatin-A4 carboxamides that mimic sulfonyl piperazines by a molecular hybridization approach: in vitro cytotoxicity evaluation and inhibition of tubulin polymerization. *ChemMedChem.* 2019;14:2052–2060.
- 28 Sigalapalli DK, Pooladanda V, Kadagathur M, et al. Novel chromenyl-based 2-iminothiazolidin-4-one derivatives as tubulin polymerization inhibitors: design, synthesis, biological evaluation and molecular modelling studies. *J Mol Struct.* 2021; 122, 128847.
- 29 Bala S, Kamboj S, Kajal A, Saini V, Prasad DN. 1,3,4-Oxadiazole derivatives: synthesis, characterization, antimicrobial potential, and computational studies. *Biomed Res Int.* 2014;2014, 172791.
- 30 Tokala R, Sana S, Lakshmi UJ, et al. Design and synthesis of thiazolo-carboxamide bridged β -carboline-indole hybrids: DNA intercalative Topo-II α inhibition with promising antiproliferative activity. *Bioorg Chem.* 2020;105, 104357.
- 31 (a) Wu J, Zhao M, Qian K, Lee K, Natschke S, Peng S. Novel N-(3-carboxyl-9-benzyl- β -carboline-1-yl)ethylamino acids: synthesis, anti-tumor evaluation, intercalating determination, 3D QSAR analysis and docking investigation. *Eur J Med Chem.* 2009; 44:4153–4161; (b) Tokala R, Thatikonda S, Sana S, Regur P, Godugu C, Shankaraiah N. Synthesis and in vitro cytotoxicity evaluation of β -carboline-linked 2,4-thiazolidinedione hybrids: potential DNA intercalation and apoptosis-inducing studies. *New J Chem.* 2018;42:16226–16236.
- 32 (a) Shahabadi N, Khashanian S, Purfoulad M. DNA interaction studies of a platinum (II) complex, PtCl₂(NN) (NN = 4,7-dimethyl-1,10-phenanthroline), using different instrumental methods. *Spectrochim Acta.* 2009;72:757–761; (b) Tokala R, Thatikonda S, Vanteddu US, Sana S, Godugu C, Shankaraiah N. Design and synthesis of DNA-interactive β -carboline-oxindole hybrids as cytotoxic and apoptosis-inducing agents. *ChemMedChem.* 2018;13:1909–1922.
- 33 Kelly JM, Tossi AB, Mcconnell DJ, Ohui-gin C. A study of the interactions of some polypyridylruthenium(II) complexes with DNA using fluorescence spectroscopy, topoisomerisation and thermal denaturation. *Nucleic Acids Res.* 1985;13:6017–6034.
- 34 (a) Tokala R, Mahajan S, Kiranmai G, et al. Development of β -carboline-benzothiazole hybrids via carboxamide formation as cytotoxic agents: DNA intercalative topoisomerase II α inhibition and apoptosis induction. *Bioorg Chem.* 2021;106, 104481; (b) Metcalfe C, Rajput C, Thomas JA. Studies on the interaction of extended terpyridyl and triazine metal complexes with DNA. *J Inorg Biochem.* 2006;100: 1314–1319.
- 35 Schrödinger Release 2019-1: Maestro, Schrödinger, LLC, New York, NY, 2019.
- 36 Cormier A, Marchand M, Ravelli RB, Knossow M, Gigant B. Structural insight into the inhibition of tubulin by vinca domain peptide ligands. *EMBO Rep.* 2008;9: 1101–1106.
- 37 (a) Rieger AM, Nelson KL, Konowalchuk JD, Barreda DR. Modified annexin V/propidium iodide apoptosis assay for accurate assessment of cell death. *J Vis Exp.* 2011;50:2597; (b) Tokala R, Bale S, Janrao IP, et al. Synthesis of 1,2,4-triazole-linked urea/Thiourea conjugates as cytotoxic and apoptosis inducing agents. *Bioorg Med Chem Lett.* 2018;28:1919–1924.
- 38 Johnpeter JP, Gupta G, Kumar JM, Srinivas G, Nagesh N, Therrien B. Biological studies of chalcogenolato-bridged dinuclear half-sandwich complexes. *Inorg Chem.* 2013;52:13663–13673.
- 39 Desbene S, Renault SG. Drugs that inhibit tubulin polymerization: the particular case of podophyllotoxin and analogues. *Curr Med Chem Anticancer Agents.* 2002;2:71–90.
- 40 Tan C, Liu J, Chen L, Shi S, Ji L. Synthesis, structural characteristics, DNA binding properties and cytotoxicity studies of a series of Ru(III) complexes. *J Inorg Biochem.* 2008;102:1644–1653.